Phys Chem Minerals (2010) 37:1–9
DOI 10.1007/s00269-009-0305-3

ORIGINAL PAPER

Structural change in lead fluorapatite at high pressure

Michael E. Fleet · Xi Liu · Sean R. Shieh

Received: 12 November 2008 / Accepted: 15 April 2009 / Published online: 1 May 2009

Abstract The structure of lead fluorapatite [PbFAP; $Pb_{10}(PO_4)_6F_2$], crystallized from the melt in a platinum capsule at 1,000°C and 1 atm, has been investigated by single-crystal X-ray diffraction. Crystal data are $a = 9.7638$ (6), $c = 7.2866$ (4) Å, space group $P6_3/m$, $R = 0.043$, $R_w = 0.034$. We have also studied the compressional behaviour of the *c*-axis channel of PbFAP up to 9 GPa at 25°C, using a diamond-anvil cell, synchrotron X-radiation, and Rietveld powder structure refinement. Pressure–volume data for the channel polyhedron of PbFAP fitted to the third-order Birch–Murnaghan equation resulted in $K_T = 33.2 \pm 1.2$ GPa when K_T' is fixed at 4. The *c*-axis channel of PbFAP is about twice as compressible as the unit-cell volume of PbFAP and the channel of calcium apatites. This is attributed to the anomalous narrowing of the channel of PbFAP with increase in confining pressure. Flexibility of the apatite channel is a key factor in the scavenging of toxic heavy metals by calcium apatites.

Keywords Lead fluorapatite · Crystal structure · Compressibility · Synchrotron X-ray diffraction · Isothermal bulk modulus · Environment

Introduction

Apatite compounds have the structural formula $M1_2M2_3(BO_4)_3X$, where M1 and M2 are large cations [Na^+, Ag^+, Ca^{2+}, Sr^{2+}, Pb^{2+}, and rare-earth elements (REE^{3+})], B metalloids (P^{5+}, C^{3+}, S^{6+}, Si^{4+}, As^{5+}, and V^{5+}), and X halides or oxy-anions [$(OH)^-$, F^-, Cl^-, $(CO_3)^{2-}$, $(HCO_3)^-$, O^{2-}, H_2O and other small neutral molecules, and vacancies] (Pan and Fleet 2002; White and Dong 2003; White et al. 2005). The calcium phosphate apatites, particularly hydroxyapatite (HAP) and fluorapatite (FAP), have importance in geochemistry, biology, agriculture, and materials science (e.g. Ma et al. 1993; Miyake et al. 1986; Pan and Fleet 2002; Elliott 2002; Fleet and Liu 2007a, b). They are the ore minerals for phosphorus and agricultural phosphates, and carbonated HAP is by far the most important biomineral, accounting for up to about 65% of cortical bone and 97% of dental enamel. Calcium apatites also readily accommodate minor-to-major amounts of large cations and, therefore, are candidate phases for the containment of high-level nuclear waste and remediation of lead contamination in soils (Kim et al. 2005). The crystal chemistry and properties of lead apatites have been of interest since Suzuki et al. (1984) reported the extensive cation exchange of Ca^{2+} in HAP by Pb^{2+} cations in aqueous solution at low pH and room temperature. Pyromorphite (lead chlorapatite) is associated with the final step of the lead cycle in roadside ecosystems (Nriagu 1984), and more recently lead hydroxyapatite [PbHAP; ideally $Pb_{10}(PO_4)_6(OH)_2$] has been identified as a corrosion product of lead pipes in a municipal water supply (Peters et al. 1999).

Powder X-ray diffraction studies have confirmed that lead fluorapatite [PbFAP; ideally $Pb_{10}(PO_4)_6F_2$] adopts the hexagonal $P6_3/m$ type structure of apatite (Belokoneva et al. 1982; Suzuki et al. 1984; Miyake et al. 1986; Kim et al. 2000; Badraoui et al. 2006), although details remain unclear. In this structure, isolated PO_4 tetrahedra centred at $z = 1/4,3/4$ are linked by Pb1 in ninefold (6 + 3) coordination and Pb2 in an irregular sevenfold (6 + 1) coordination (Fig. 1). A prominent feature is the large *c*-axis

M. E. Fleet (✉) · X. Liu · S. R. Shieh
Department of Earth Sciences,
University of Western Ontario,
London, ON N6A 5B7, Canada
e-mail: mfleet@uwo.ca

channel which accommodates the F anion in PbFAP, and a variety of X anion components in other apatites. The apatite channel of PbFAP is defined by triclusters of Pb2 cations at $z = 1/4,3/4$. In FAP, the F anion is located on the *c*-axis at $z = 1/4,3/4$ in the centre of a tricluster of Ca2 cations. The z coordinate of the F anion in PbFAP was assumed to be 1/4 in the X-ray single-crystal study of Belokoneva et al. (1982), and 1/2 in the neutron powder diffraction study of Kim et al. (2000). However, Badraoui et al. (2006) found that in (Pb,Sr)FAP fluorine is actually displaced along the *c*-axis in between $z = 1/4$ and 1/2, occupying a split atom position with occupancy of 0.5: a similar displacement occurs for the OH oxygen in PbHAP (Bigi et al. 1989; Badraoui et al. 2001). The trigonally distorted octahedron formed by the Pb2 cations in the channel wall (Fig. 1), and presently referred to as the "channel polyhedron", is a convenient measure of one-half of the channel volume.

We have recently investigated the compressional behaviour of lead fluorapatite up to about 16.7 GPa at 300 K, using a diamond-anvil cell and synchrotron X-ray diffraction (Liu et al. 2008), observing that PbFAP is much more compressible than FAP and HAP and approximately elastically isotropic. In the present paper, we refine the PbFAP structure using single-crystal X-ray diffraction at room temperature and pressure, and investigate the compressional behaviour of its *c*-axis channel.

Experimental procedures

Lead fluorapatite (PbFAP; experiment LM24) was synthesized at 1 atm in a conventional muffle furnace. The starting material was a stoichiometric mixture of lead fluoride and lead orthophosphate encapsulated in a sealed platinum tube. The experimental temperature was set initially at 1,100°C, i.e. 2° above the 1 atm solidus of lead fluorapatite (Podsiadlo 1990), for 3 h then decreased with a ramp of 1 °C/min to 1,000°C, and maintained at 1,000°C for 10 h. The experiment was terminated by quenching the capsule in cold water. We also synthesized PbFAP crystals at 700 and 850°C at 1 atm, and 950°C and 0.14 GPa in a hydrothermal apparatus, and 850°C and 1.0 GPa in a piston cylinder apparatus. Crystal products were characterized by optical microscopy, powder X-ray diffraction (Rigaku D/MAX-B rotating anode system; Co $K\alpha$ X-radiation), electron probe micro-analysis (EPMA; JEOL JXA-8600), and Fourier transform infrared spectroscopy (FTIR; Nicolet Nexus 670 FTIR spectrometer).

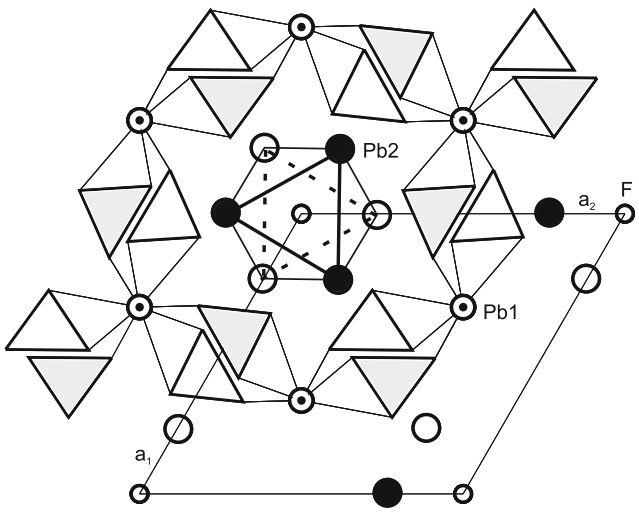

Fig. 1 Structure of lead fluorapatite (PbFAP) identifying polyhedron formed by Pb2 cations in apatite channel wall: *open Pb2 circles* are at height $z = 1/4$ and *filled circles* are at $z = 3/4$; *triangles* are PO_4 tetrahedra centred at $z = 1/4$ (*open*) and $z = 3/4$ (*shaded*)

Single-crystal measurements were made at room temperature and pressure with a Bruker-Nonius Kappa CCD diffractometer and graphite-monochromatized Mo $K\alpha$ X-radiation (50 kV, 32 mA, $\lambda = 0.7107$ Å). The COLLECT software (Bruker-Nonius 1997) was used for unit-cell refinement and data collection. The reflection data were processed with SORTAV-COLLECT, using an empirical procedure for absorption correction. Structure refinements were made with LINEX77 (Coppens 1977). Scattering factors for neutral atomic species and values of the anomalous scattering factors f' and f'' were taken, respectively, from Tables 2.2A and 2.3.1 of the *International Tables for X-ray Crystallography* (Ibers and Hamilton 1974). Relevant experimental details are given in Table 1, final parameters in Table 2, and selected bond distances in Table 3.

High-pressure angle dispersive X-ray diffraction experiments were conducted using a symmetrical diamond-anvil cell at beamline X17C, National Synchrotron Light Source, Brookhaven National Laboratory. A T301 stainless steel plate with an initial thickness of 250 μm was used as gasket. The central area of the plate was pre-indented to a thickness of about 40 μm, and a hole of 150 μm in diameter was drilled through it. The pressure medium was a 4:1 methanol–ethanol mixture. A finely ground powder of lead fluorapatite from experiment LM24 and two ruby spheres were loaded with the pressure medium, one sphere near the centre and the other close to the edge of the sample chamber. The experimental pressure was determined by the ruby fluorescence method (Mao et al. 1978). The incident synchrotron radiation beam was monochromatized to a wavelength of 0.4066 Å and collimated to a beam size at the sample of $\sim 25 \times 20$ μm^2. X-ray powder diffraction patterns were collected at room temperature for 10–15 min using an imaging plate, initially at room pressure and then sequentially at intervals of increasing pressure up to 16.8 GPa. Finally, the pressure was reduced to 1.60 GPa

Table 1 Experimental details for single-crystal X-ray structure

Experiment	LM24
Crystal	xt392
Crystal size (mm)	0.03 × 0.05 × 0.08
Crystal shape	Prism
a (Å)	9.7638 (6)
c (Å)	7.2866 (4)
Space group	$P6_3/m$
Formula weight	2679.7
Density (g/cm^3)	7.397
Reflections, unique	495
$(I < 3\sigma_{(I)})$	162
$R_{(I)}$	0.036
$R_{(I),w}$	0.046
Refined parameters	26
μ (cm^{-1})	702.1
R	0.043
R_w	0.034
s	1.01
g ($\times 10^4$)	0.42 (2)
$\Delta\rho$ (eÅ^{-3}) (+)	3.3
(−)	2.2

Table 2 Positional and isotropic thermal parameters (Å^2) from single-crystal study $U_{eq} = (1/3)\ \Sigma_i\Sigma_j\ U^{ij}\ a^i a^j\ a_i{\cdot}a_j$

	Site occupancy	x	y	z	U,U_{eq}
Pb1	1.0	2/3	1/3	0.0031 (2)	0.0204 (7)
Pb2	1.0	0.0040 (1)	0.2357 (1)	0.25	0.0253 (4)
P	1.0	0.3819 (7)	0.4063 (7)	0.25	0.015 (1)
O1	1.0	0.484 (2)	0.328 (1)	0.25	0.010 (3)
O2	1.0	0.487 (2)	0.586 (2)	0.25	0.020 (4)
O3	1.0	0.273 (1)	0.356 (1)	0.081 (1)	0.020 (3)
F	1.0	0	0	0.461 (4)	0.030 (9)

(experiment A17; Table 3) to demonstrate reversibility of the effects of compression. CeO_2 was used to calibrate the sample to detector distance as well as the orientation of the detector. The two-dimensional ring patterns were integrated off-line to give conventional one-dimension powder pattern profiles using FIT2D (Hammersley 1996). Powder structure refinements were made using GSAS (Larson and Von Dreele 2000), and are reported in Table 4. The diffraction patterns were limited to a maximum 2θ of 14.0° by the diamond-anvil cell. Starting parameters for the seven-atom structure were taken from the present single-crystal study (Table 2), but only the z coordinate of Pb1 and x and y of Pb2 were varied in the least-squares refinements, along with the unit-cell parameters, a five-parameter function for the background, and three peak profile parameters.

Results and discussion

The crystal products were colourless and transparent, and the FTIR spectra suggested that they were essentially hydroxyl ion free. The EPMA for LM24 was slightly low in Pb and F (Liu et al. 2008) but these discrepancies are readily attributable to the difficulty in analysing light elements in a matrix dominated by lead. On the other hand, the single-crystal X-ray structure refinement resulted in site occupancies of 0.985 (5) for Pb1 and 0.993 for Pb2. Therefore, the stoichiometric $Pb_{10}(PO_4)_6F_2$ composition was assumed for both single-crystal and powder structure refinements.

The bond distances for the room-pressure single-crystal structure refinement of PbFAP are comparable to those for the recent single-crystal study of lead oxyapatite (Krivovichev and Burns 2003), taking into account that the X anion species (F^- and O^{2-}, respectively) are located at quite different heights in the apatite channel (Table 3). The P–O bond distances for PbFAP are similar to those of calcium apatites, which are generally within the range 1.52–1.54 Å (Hughes et al. 1989; Fleet et al. 2004). Interestingly, the Pb–O bond distances in PbFAP do not show the systematic increase over the corresponding distances in FAP (Table 3) expected from the large differences in effective ionic radii of Pb^{2+} and Ca^{2+}. The differences in bond distances between PbFAP and FAP range from +0.04 to +0.27 Å for Pb1–O and +0.01 to +0.24 Å for Pb2–O, compared with theoretical differences of +0.17 Å for the ninefold coordination of Pb1 and +0.19 Å for the sixfold coordination of Pb2 (Shannon 1976). However, the +0.15 and +0.17 Å differences for the mean bond distances of Pb1–O and Pb2–O, respectively, are in much better agreement with the effective ionic radii.

The room-pressure results for PbHAP in Table 3 were obtained by powder X-ray diffraction refinement assuming a rigid PO_4 tetrahedron (Brückner et al. 1995). Because the lead atoms dominate the X-ray scattering, it is not possible to obtain accurate values for the parameters of the light atoms in lead apatites from powder data using conventional source X-rays: e.g. the refined powder structure of a lead–strontium fluorapatite solid solution of composition $(Pb_9Sr_1)_{10}(PO_4)_6F_2$ (Badraoui et al. 2006) resulted in P–O distances of 1.19–1.56 Å. The present structure refinements made with synchrotron radiation powder diffraction data collected in situ at high pressure failed to converge when the light atoms (P, O, and F) were included. However, our partial structure refinement procedure, using structural parameters for the light atoms from the single-crystal study, has located the heavy lead atoms and yielded direct evidence of pressure-induced structural change in the apatite channel. The powder patterns are accurately

Table 3 Bond distances (Å) and angles (°)

Bond/angle		PbFAP[a]	FAP[b]	PbOAP[c]	PbHAP[d]
a (Å)		9.7638 (6)	9.398 (3)	9.8650 (3)	9.866 (3)
c (Å)		7.2866 (4)	6.878 (2)	7.4306 (3)	7.426 (2)
Pb1–O1	×3	2.51 (1)	2.40	2.56	2.67
Pb1–O2^{I}	×3	2.73 (1)	2.46	2.66	2.62
Pb1–O3^{I}	×3	2.85 (1)	2.81	2.94	3.01
Mean		2.70	2.55	2.72	2.77
Pb2–O1^{II}		2.93 (1)	2.70	2.95	2.89
Pb2–O2^{III}		2.38 (2)	2.37	2.44	2.54
Pb2–O3^{IV}	×2	2.59 (1)	2.35	2.60	2.59
Pb2–O3^{V}	×2	2.64 (1)	2.50	2.64	2.62
Mean		2.63	2.46	2.64	2.64
Pb2–F(O,OH))		2.75 (2)	2.31	2.58	2.90
Pb2–F(O,OH)		3.11 (2)		–	–
P–O1		1.53 (2)	1.54	1.56	1.51
P–O2		1.53 (2)	1.54	1.57	1.51
P–O3	×2	1.54 (1)	1.53	1.55	1.51
Mean		1.53	1.54	1.55	1.51
O1–P–O2		109.9 (8)	111.0	109.4	109.5
O1–P–O3	×2	111.0 (5)	111.1	111.9	109.5
O2–P–O3	×2	109.1 (6)	108.0	108.6	109.5
O3–P–O3^{VI}		106.7 (8)	107.4	106.4	109.5

(I) $1 - x, 1 - y, -z$; (II) $1 - y, x - y, z$; (III) $1 - x + y, 1 - x, z$; (IV) $1 + x, y, z$; (V) $1 + x - y, x, -z$; (VI) $x, y, \frac{1}{2} - z$

[a] Lead fluorapatite, single crystal, this study

[b] Fluorapatite, single crystal (Hughes et al. 1989)

[c] Lead oxyapatite, single crystal Krivovichev and Burns 2003)

[d] Lead hydroxyapatite, powder, rigid body PO_4 refinement (Brückner et al. 1995)

Table 4 Powder structure refinements at high pressure and 25°C

Expt.	Pressure (GPa)	*a* (Å)	*c* (Å)	*V* (Å^3)	R_p	Pb1[a]	Pb2	
						z	*x*	*y*
A2	2.44	9.643 (2)	7.188 (1)	578.9 (2)	0.014	0.994 (3)	0.000 (3)	0.231 (2)
A3	2.96	9.634 (2)	7.181 (2)	577.2 (3)	0.014	0.994 (4)	0.003 (4)	0.232 (2)
A4	4.00	9.592 (2)	7.150 (2)	569.7 (3)	0.014	0.993 (5)	0.999 (4)	0.227 (2)
A5	4.99	9.554 (2)	7.125 (2)	563.2 (4)	0.014	0.986 (3)	0.002 (5)	0.229 (2)
A6	5.89	9.522 (2)	7.102 (2)	557.7 (3)	0.016	0.990 (3)	0.002 (5)	0.228 (2)
A7	7.20	9.484 (2)	7.077 (2)	551.3 (3)	0.015	0.989 (3)	0.999 (4)	0.225 (2)
A8	7.99	9.462 (2)	7.061 (2)	547.4 (3)	0.015	0.986 (3)	0.998 (4)	0.223 (2)
A9	9.05	9.429 (2)	7.038 (2)	541.9 (3)	0.015	0.986 (3)	0.997 (4)	0.224 (2)
A17[b]	1.60	9.697 (2)	7.226 (1)	588.4 (2)	0.032	0.990 (2)	0.001 (3)	0.232 (1)

[a] Other structure parameters are given in Table 2

[b] Reversal experiment

reproduced because the scattering contributions associated with the parameter shifts for the light atoms are relatively small. Lead atoms account for about 75% of F_{000} (which is 1,120 electron units for ideal stoichiometry), and their scattering contributions totally dominate the X-ray diffraction powder pattern of PbFAP at high 2θ (below 3.0 Å). Also, interference from overlapped powder lines was minimal. There were about 45 reflections out to 1.665 Å, with ten pairs symmetry-equivalent in the higher hexagonal Laue symmetry (6/*mmm*).

The present results for the effect of pressure on the unit-cell parameters and volume of PbFAP agree closely with the recent measurements of Liu et al. (2008) (Fig. 2; Table 4). Although powder diffraction data were collected up to 16.8 GPa, we also found that measurements beyond 9–10 GPa were not quantitative, due to solidification of the methanol–ethanol pressure medium at ~10 GPa. Nevertheless, the extended results in Liu et al. (2008) and this study do confirm that apatite-structure PbFAP is stable up to ~17 GPa at 25°C. Also, the results for experiment A17

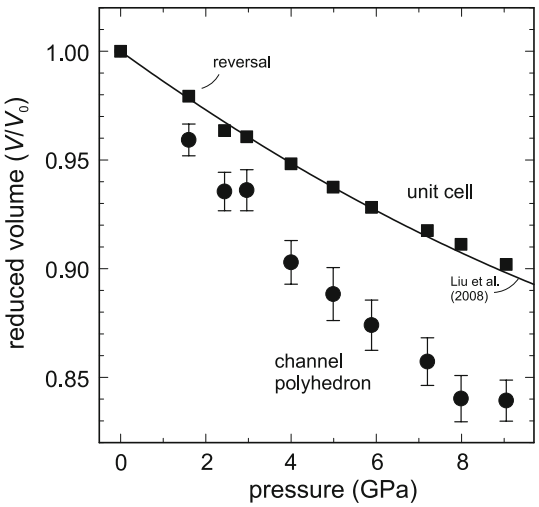

Fig. 2 Reduced volume (V/V_0) plot showing compression of the unit cell and channel polyhedron of PbFAP: note that the apatite channel is twice as compressible as the overall structure; departure from smooth trends beyond 9 GPa reflects loss of hydrostatic condition; *regression line* is result of Liu et al. (2008); error in pressure estimates is within symbol size

(Table 4), which are plotted at 1.6 GPa in Figs. 2 and 3, show that the elastic behaviour of PbFAP is completely reversible after compression to 16.8 GPa.

The pressure–volume data at pressures below 10 GPa were fitted to the third-order Birch–Murnaghan equation, which yielded an isothermal bulk modulus (K_T) of 57.2 ± 0.8 GPa and first pressure derivative (K_T') of 8.7 ± 0.4. With K_T' fixed at 4, the derived K_T is 68.4 ± 0.3 GPa in good agreement with Liu et al. (2008). A plot of normalized pressure versus Eulerian strain (F–f plot; Angel 2000) yielded values of $K_0 = 58 \pm 2$ GPa and $K_0' = 8 \pm 2$, and suggested that the third-order Birch–Murnaghan equation was appropriate. The present value for the isothermal bulk modulus of PbFAP is approximately two-thirds of the isothermal bulk moduli of FAP, HAP, and chlorapatite (Sha et al. 1994; Brunet et al. 1999; Comodi et al. 2001; Matsukage et al. 2004). Thus, PbFAP is significantly more compressible than the calcium apatites in the investigated pressure range. These differences in elastic behaviour of PbFAP and the calcium apatites were attributed in Liu et al. (2008) to the different ionic size and bonding character of the large cations, Pb^{2+} and Ca^{2+}.

The literature studies on FAP have revealed a weak compressional anisotropy (Sha et al. 1994; Brunet et al. 1999; Comodi et al. 2001; Matsukage et al. 2004), with the unit-cell axial ratio *a*/*c* decreasing by about 0.7% from 0 to 7 GPa in Comodi et al. (2001) (Fig. 3b). Liu et al. (2008) concluded that PbFAP is essentially isotropic because *a*/*c* appeared to be invariant. Nevertheless, the present precise measurements do suggest a very weak elastic anisotropy (Fig. 3a), with *a*/*c* decreasing about 0.2% to 10 GPa. The X-ray diffraction powder patterns for the room-pressure sample in this study resulted in anomalously high unit-cell parameters (No. 2 in Table 5). Therefore, room-pressure unit-cell parameters for the powder sample of PbFAP were obtained by regression of the separate high-pressure distributions for *a*, *c*, volume, and *a*/*c* (No. 1 in Table 5): note that experiment A17 (Table 4; Fig. 3a) shows that the compression of PbFAP is completely reversible. The unit-cell volume at 1 bar derived by regression corresponds quite well with that from the single-crystal study, 601.58 (6) $Å^3$, which was the value used for V_0 in the bulk modulus calculation. The discrepancies in the values for axial ratio (*a*/*c*) in Table 5 may be simply an artefact of different determination procedures. However, the difference between the cell edges of the decompressed powder and single crystal (1 and 4 in Table 5) must be regarded as significant, and reveal a decrease in *a* and increase in *c* in the single crystal (the uncompressed sample). Similar relative shifts in *a* and *c* are evident for the two uncompressed powder samples (2 and 3 in Table 5). We speculate that this trend reflects damage to the PbFAP crystals during quenching from the high temperature of crystal synthesis, with subsequent annealing of this damage at high pressure. It is well known that irradiation of fragile crystals results in increase in unit-cell parameters. Volume increases up to 0.8% have been documented for protein crystals (Ravelli et al. 2002), and attributed to change induced by thermal expansion during irradiation followed by cooling to ambient conditions.

The progressive reduction in volume of the channel polyhedron with increase in pressure (Fig. 2) represents the combined effects of decrease in volume of the unit cell and shifts in the positional coordinates *x* and *y* of Pb2. The effect of the latter has to be very significant because the channel polyhedron is much more compressible than the unit cell (Fig. 2). Moreover, Pb2 is located on the symmetry plane so that the height of the channel polyhedron is fixed, and equal to *c*/2. Therefore, the structural component of the volume compression must be related exclusively to progressive shift of the Pb2 cations towards the *c*-axis; i.e. towards the centre of the apatite channel. The progressive narrowing of the apatite channel, and consequent change in shape of the channel polyhedron, is reflected in progressive increase in the distortion parameter mean quadratic elongation (λ). Noting that the channel polyhedron is a stretched trigonally distorted octahedron, λ is given by:

$$\lambda = \frac{1}{6}\sum_{i=1}^{6}(\ell_i/\ell_0)^2,$$

where ℓ_0 is the bond length for the ideal, undistorted octahedron equal in volume to the octahedron in question

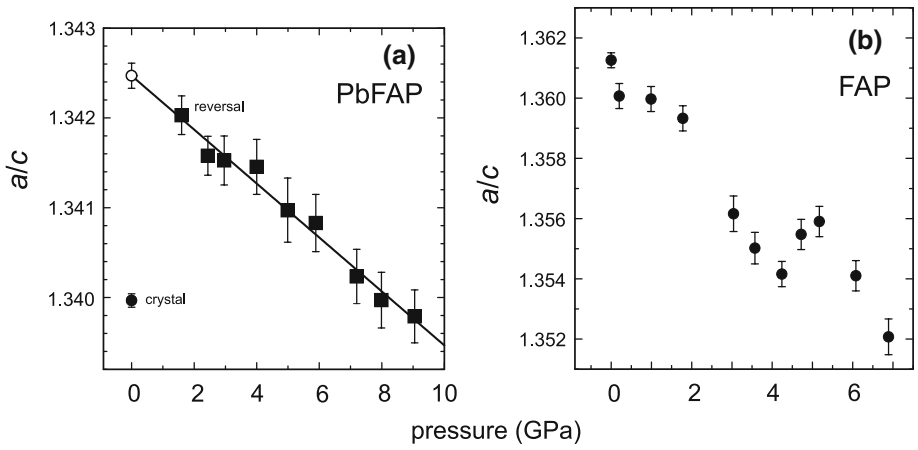

Fig. 3 Variation of unit-cell axial ratio (*a*/*c*) with pressure revealing a very weak elastic anisotropy in PbFAP compared with FAP (Comodi et al. 2001): room-pressure value for powder sample (*filled circle*) represents extrapolation of high-pressure data; error in pressure estimates is within symbol size

Table 5 Comparison of 1 bar unit-cell parameters

Sample	*a* (Å)	*c* (Å)	Volume (Å^3)	*a*/*c*	Δ*a* (%)	Δ*c* (%)
Powder samples						
(1)[a]	9.767 (5)	7.276 (2)	601.1 (4)	1.3425 (1)	–	–
(2)[b]	9.787 (1)	7.309 (1)	606.3 (2)	1.3390	+0.020	+0.033
(3)[c]	9.757 (3)	7.283 (4)	600.4 (3)	1.3397	−0.010	+0.007
Single crystal						
(4)[d]	9.7638 (6)	7.2866 (4)	601.58 (6)	1.3400	−0.003	+0.011

[a] Compressed, by extrapolation of *a*, *c*, *V*, and *a*/c

[b] Untreated, this study

[c] Untreated, Liu et al. (2008)

[d] Crystal xt392, Table 1

(Robinson et al. 1971). As shown in Fig. 4, λ for the channel polyhedron increases linearly with increase in confining pressure, within error of determination. Minor departures from isotropic compression (Fig. 3a) and lack of the precise values for the *z* coordinate of the F anion both contribute to uncertainty in the values of λ but are not significant in influencing the overall trends.

A more direct demonstration of the influence of the shifts in *x* and *y* coordinates on reduction in the volume of the channel polyhedron and narrowing of the apatite channel is afforded by the decrease in the normal distance of Pb2 to the *c*-axis at constant unit-cell volume (R_X; Fig. 4). The channel polyhedron is terminated by the two equilateral triangular faces formed by the trigonal clusters of Pb2 cations (Fig. 1). Therefore, R_X is a measure of the change in width of the apatite channel. Figure 4 shows that the normalized values of R_X decrease linearly with increase in confining pressure. Since *a* and *c* have been held constant, the only variable parameters constricting the width of the apatite channel are the atomic coordinates *x* and *y* of Pb2.

The compressibility data for the channel polyhedron of PbFAP correspond to a bulk modulus of $K_T = 33.2 \pm 1.2$ GPa when K_T' is fixed at 4. Thus, the channel polyhedron of PbFAP is almost two times weaker than the bulk sample and three times weaker than FAP. The compressibilities of PbFAP and FAP are compared in Fig. 5. Comodi et al. (2001) obtained in situ single-crystal structures at 0.0001, 3.04, and 4.72 GPa, from which they extracted data for the compressibility of the polyhedral volumes of the P, Ca1, and Ca2 positions: the derived polyhedral bulk moduli were 270, 100, and 86 GPa for P, Ca1, and Ca2, respectively. We presently calculate the compressibility of the channel polyhedron of FAP to be intermediate between that of the Ca1 and Ca2 polyhedra (Fig. 5). Our value for the reduced polyhedral volume is in agreement with that obtained by Comodi et al. (2001), who used the volume of the trigonal prism formed by unit translation of the tricluster of Ca2 cations along [001]. The *c*-axis channel of PbFAP is twice as compressible as that of FAP (and, presumably, of other calcium apatites as well). The comparison between PbFAP and FAP is even more striking when compressibility differences with the corresponding unit-cell volumes are compared: e.g. at 4.7 GPa, the channel polyhedron is 82% more compressible than the unit-cell volume for PbFAP but only 23% more compressible for FAP (Fig. 5). This is no doubt attributable to

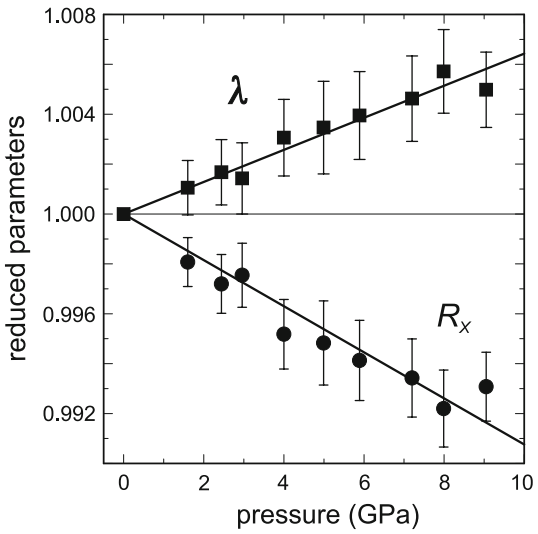

Fig. 4 Progressive linear increase in the normalized distortion parameter mean quadratic elongation (λ) for the channel polyhedron and decrease in channel width (proportional to R_X), both associated with the shift of Pb2 cations towards the *c*-axis. Functions plotted are (λ/λ_0) and $(1 - ((1 - (R_X/R_{X,0}))/5))$, where R_X is calculated at constant unit-cell volume; room-pressure single-crystal structure used as reference; error in pressure estimates is within symbol size

the much greater polarizability of Pb^{2+} (38.3 $Å^3$ compared with 5.2 $Å^3$ for Ca^{2+}) (Pohl 1978).

Although the channel polyhedron accounts for only about 10% of the unit-cell volume of apatites (there are two polyhedra per unit cell), the apatite channel is of fundamental importance to the integrity and chemical interaction

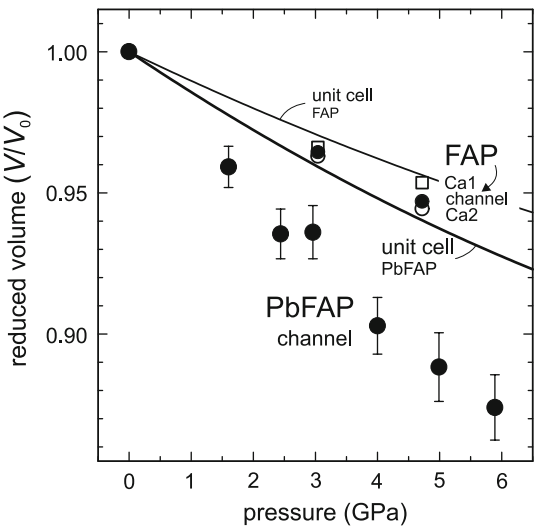

Fig. 5 Reduced unit-cell and channel polyhedral volumes for PbFAP (*thick line* and *filled circles* with error bars, respectively) compared with results for FAP from Comodi et al. (2001), who also obtained polyhedral volumes for Ca1 (*open squares*) and Ca2 (*open circles*): note that not only is PbFAP much softer than FAP, but the relative compression of its *c*-axis channel is disproportionately greater

of the apatite structure. However, notwithstanding the marked differences in compressibility, there are no known differences in the persistence of FAP and PbFAP under very high pressure conditions at room temperature. FAP apatites did not show evidence of pressure-induced amorphization up to 25 GPa by spectroscopic studies (Williams and Knittle 1996) and 18.3 GPa by diffraction studies (Brunet et al. 1999). In the present study on PbFAP, peak broadening was noticeable at 11.3 GPa and increased progressively to the maximum pressure investigated (16.8 GPa), but this effect was completely reversible on reduction of the pressure. However, there may be significant differences in the pressure stability of apatites at high temperature: e.g. reaction of the PbFAP product from experiment LM24 at 10 GPa and 1,200°C resulted in a new phase with a derivative barium phosphate [$Ba_3(PO_4)_2$] structure (work in progress). This phase transformation is likely driven by loss of the channel volatile content at high temperature, rather than collapse of the apatite channel at high pressure.

Phosphate apatites are ideal candidate phases for containment of radioactive waste and remediation of toxic waste contamination. They have a low solubility under surface conditions and are stable to high temperature and pressure, and yet are sufficiently reactive to anneal radiation damage under moderate-temperature hydrothermal conditions. Moreover, the apatite structure accommodates minor-to-major amounts of foreign cations and anions through solid solution at high temperature and exchange at low temperature. Different sized M1 and M2 cations and channel anions are readily accommodated by rotation and translation of the PO_4 tetrahedra (Fig. 1). The adaptability of the apatite structure is well illustrated by the differential expansion of the M–O bond distances when Pb substitutes for Ca (Table 3). Also, in near-end-member carbonate apatite the carbonate ions are ordered along the apatite channel at $z \approx 0.5$, with a possible location at $z \approx 0.0,1.0$ unoccupied (Fleet and Liu 2003). The phosphate groups are displaced slightly from ideal HAP positions to dilate the apatite channel in the immediate vicinity of the bulky carbonate ion, and constrict it above and below. Although the channel constituents of hexagonal apatites with mixed X anion occupancy are disordered within the overall structure, individual channel species are probably locally ordered in *c*-axis domains (Elliott 2002). Furthermore, cations and anions introduced by complex, charge-balanced substitutions may be present as coupled defect clusters within a calcium apatite matrix, as in Na-bearing carbonate apatites (Fleet and Liu 2007b). Even though PbFAP is elastically much softer than calcium apatites, and Pb–O bonds have more covalent character than Ca–O bonds, and Pb^{2+} and Ca^{2+} are quite different in size, divalent lead can be scavenged from acidic aqueous

solutions by nanoscale particles of calcium apatites. The flexible apatite channel has an important role here in providing structural pathways for exchange of the M1 and M2 cations.

Acknowledgments We thank two reviewers for helpful comments, Michael Jennings for collection of the X-ray reflection data, Jingzhu Hu for assistance with the synchrotron X-ray diffraction experiments, and the Natural Sciences and Engineering Research Council of Canada for financial support.

References

Angel RJ (2000) Equations of state. In: Hazen RM, Downs RT (eds) High-temperature and high-pressure crystal chemistry. Reviews in mineralogy and geochemistry, vol 41. Mineralogical Society of America, Washington DC, pp 35–59

Badraoui B, Bigi A, Debbabi M, Gazzano M, Roveri N, Thouvenot R (2001) X-ray powder diffraction and solid state NMR investigations in cadmium-lead hydroxyapatites. Eur J Inorg Chem 2001:1261–1267. doi:10.1002/1099-0682(200105)2001:5<1261::AID-EJIC1261>3.0.CO;2-S

Badraoui B, Aissa A, Bigi A, Debbabi M, Gazzano M (2006) Structural investigations of lead-strontium fluoroapatites. J Solid State Chem 179:3065–3072. doi:10.1016/j.jssc.2006.06.001

Belokoneva EL, Troneva EA, Dem'yanets LN, Duderov NG, Belov NV (1982) Crystal structure of synthetic fluoropyromorphite $Pb_5(PO_4)_3F$. Sov Phys Crystallogr 27:476–477

Bigi A, Ripamonti A, Brückner S, Gazzano M, Roveri N, Thomas SA (1989) Structure refinements of lead-substituted calcium hydroxyapatite by X-ray powder fitting. Acta Crystallogr B 45:247–251. doi:10.1107/S0108768189001928

Brückner S, Lusvardi G, Menabue L, Saladini M (1995) Crystal structure of lead hydroxyapatite from powder X-ray diffraction data. Inorg Chim Acta 236:209–212. doi:10.1016/0020-1693(95)04636-N

Bruker-Nonius (1997) COLLECT Software. Bruker-Nonius, Delft, The Netherlands

Brunet F, Allan DR, Redfern SAT, Angel RJ, Miletich R, Reichmann HJ, Sergent J, Hanfland M (1999) Compressibility and thermal expansivity of synthetic apatites, $Ca_5(PO_4)_3X$ with X=OH, F and Cl. Eur J Mineral 11:1023–1035

Comodi P, Liu Y, Zanazzi PF, Montagnoli M (2001) Structural and vibrational behaviour of fluorapatite with pressure. Part I: in situ single-crystal X-ray diffraction investigation. Phys Chem Miner 28:219–224. doi:10.1007/s002690100154

Coppens P (1977) LINEX77. State University of New York, Buffalo

Elliott JC (2002) Calcium phosphate biominerals. In: Kohn MJ, Rakovan J, Hughes JM (eds) Phosphates: geochemical, geobiological and material importance. Reviews in mineralogy and geochemistry, vol 48. Mineralogical Society of America, Washington DC, pp 427–453

Fleet ME, Liu X (2003) Carbonate apatite type A synthesized at high pressure: new space group ($P\bar{3}$) and orientation of channel carbonate ion. J Solid State Chem 174:412–417. doi:10.1016/S0022-4596(03)00281-0

Fleet ME, Liu X (2007a) Hydrogen-carbonate ion in synthetic high-pressure apatite. Am Mineral 92:1764–1767. doi:10.2138/am.2007.2716

Fleet ME, Liu X (2007b) Coupled substitution of type A and B carbonate in sodium-bearing apatite. Biomaterials 28:916–926. doi:10.1016/j.biomaterials.2006.11.003

Fleet ME, Liu X, King PL (2004) Accommodation of the carbonate ion in apatite: an FTIR and X-ray structure study of crystals synthesized at 2–4 GPa. Am Mineral 89:1422–1432

Hammersley J (1996) FIT2D report. European Synchrotron Radiation Facility, Grenoble

Hughes JM, Cameron M, Crowley KD (1989) Structural variations in natural F, OH, and Cl apatites. Am Mineral 74:870–876

Ibers JA, Hamilton WC (eds) (1974) International tables for X-ray crystallography, vol IV. Kynoch Press, Birmingham

Kim JY, Fenton RR, Hunter BA, Kennedy BJ (2000) Powder diffraction studies of synthetic calcium and lead apatites. Aust J Chem 53:679–686. doi:10.1071/CH00060

Kim JY, Dong Z, White TJ (2005) Model apatite systems for the stabilization of toxic metals: II, cation and metalloid substitutions in chlorapatites. J Am Ceram Soc 88:1253–1260. doi:10.1111/j.1551-2916.2005.00136.x

Krivovichev SV, Burns PC (2003) Crystal chemistry of lead oxide phosphates: crystal structures of $Pb_4O(PO_4)_2$, $Pb_8O_5(PO_4)_2$ and $Pb_{10}(PO_4)_6O$. Z Kristallogr 218:357–365. doi:10.1524/zkri.218.5.357.20732

Larson AC, Von Dreele RB (2000) General structure analysis system (GSAS). Los Alamos National Laboratory Report LAUR 86-748

Liu X, Shieh SR, Fleet ME, Akhmetov A (2008) High-pressure study on lead fluorapatite. Am Mineral 93:1581–1584. doi:10.2138/am.2008.2816

Ma QY, Traina SJ, Logan TJ, Ryan JA (1993) In situ lead immobilization by apatite. Environ Sci Technol 27:1803–1810. doi:10.1021/es00046a007

Mao HK, Bell PM, Shaner JW, Steinberg DJ (1978) Specific volume measurements of Cu, Mo, Pt, and Au and calibration of ruby R1 fluorescence pressure gauge for 0.006 to 1 Mbar. J Appl Phys 49:3276–3283. doi:10.1063/1.325277

Matsukage KN, Ono S, Kawamoto T, Kikegawa T (2004) The compressibility of a natural apatite. Phys Chem Miner 31:580–584. doi:10.1007/s00269-004-0415-x

Miyake M, Ishigaki K, Suzuki T (1986) Structure refinements of Pb^{2+} ion-exchanged apatites by X-ray powder pattern-fitting. J Solid State Chem 61:230–235. doi:10.1016/0022-4596(86)90026-5

Nriagu JO (1984) Formation and stability of heavy metal phosphates in soils and sediments. In: Nriagu JO, Moore PB (eds) Phosphate minerals. Springer, New York, pp 318–329

Pan Y, Fleet ME (2002) Compositions of the apatite-group minerals: substitution mechanisms and controlling factors. In: Kohn MJ, Rakovan J, Hughes JM (eds) Phosphates: geochemical, geobiological and material importance, reviews in mineralogy and geochemistry, vol 48. Mineralogical Society of America, Washington DC, pp 13–49

Peters NJ, Davidson CM, Britton A, Robertson SJ (1999) The nature of corrosion products in lead pipes used to supply drinking water to the city of Glasgow, Scotland, UK. Fresenius J Anal Chem 363:562–565. doi:10.1007/s002160051247

Podsiadlo H (1990) Polymorphic transitions in the binary system lead fluorapatite [Pb10(PO4)6F2]–calcium fluorapatite. J Therm Anal 36:569–575. doi:10.1007/BF01914510 $Ca_{10}(PO_4)_6F_2$

Pohl D (1978) Electronic polarizabilities of ions in doubly refracting crystals. Acta Crystallogr A 34:574–578. doi:10.1107/S0567739478001217

Ravelli RBG, Theveneau P, McSweeney S, Caffrey M (2002) Unit-cell volume change as a metric of radiation damage in crystals of macromolecules. J Synchrotron Radiat 9:355–360. doi:10.1107/S0909049502014541

Robinson K, Gibbs GV, Ribbe PH (1971) Quadratic elongation: a quantitative measure of distortion in coordination polyhedra. Science 172:567–570. doi:10.1126/science.172.3983.567

Sha MC, Li Z, Bradt RC (1994) Single-crystal elastic constants of fluorapatite, $Ca_5(PO_4)_3F$. J Appl Phys 75:7784–7787. doi:10.1063/1.357030

Shannon RD (1976) Revised effective ionic radii and systematic studies of interatomic distances in halides and chalcogenides. Acta Crystallogr A 32:751–767. doi:10.1107/S0567739476001551

Suzuki T, Ishigaki K, Miyake M (1984) Synthetic hydroxyapatites as inorganic cation exchangers. J Chem Soc Faraday Trans I 80:3157–3165. doi:10.1039/f19848003157

White TJ, Dong Z-L (2003) Structural derivation and crystal chemistry of apatites. Acta Crystallogr B 59:1–16. doi:10.1107/S0108768102019894

White TJ, Ferraris C, Kim J, Madhavi S (2005) Apatite—an adaptive framework structure. In: Ferraris G, Merlino S (eds) Micro- and meso-porous mineral phases. Reviews in mineralogy and geochemistry, vol 57. Mineralogical Society of America, Washington DC, pp 307–373

Williams Q, Knittle E (1996) Infrared and Raman spectra of $Ca_5(PO_4)_3F_2$-fluorapatite at high pressures: compression-induced changes in phosphate site and Davydov splittings. J Phys Chem Solids 57:417–422. doi:10.1016/0022-3697(95)00285-3